atmosphere

MDPI

Article

Preliminary Findings on CO_2 Capture over APTES-Modified TiO_2

Agnieszka Wanag *, Joanna Kapica-Kozar, Agnieszka Sienkiewicz, Paulina Rokicka-Konieczna, Ewelina Kusiak-Nejman and Antoni W. Morawski

Department of Inorganic Chemical Technology and Environment Engineering, Faculty of Chemical Technology and Engineering, West Pomeranian University of Technology in Szczecin, Pułaskiego 10, 70-322 Szczecin, Poland
* Correspondence: awanag@zut.edu.pl

Abstract: In this work, the impact of TiO_2 properties on the CO_2 adsorption properties of titanium dioxide modified with 3-aminopropyltriethoxysilane (APTES) was presented. The APTES-modified TiO_2 materials were obtained by solvothermal process and thermal modification in the argon atmosphere. The prepared adsorbents were characterized by various techniques such as X-ray diffraction (XRD), Fourier transform infrared (DRIFT), thermogravimetric analysis and BET specific surface area measurement. CO_2adsorption properties were measured at different temperatures (0, 30, 40, 50 and 60 °C). Additionally, the carbon dioxide cyclic adsorption-desorption measurements were also investigated. The results revealed that modifying TiO_2 with APTES is an efficient method of preparing CO_2 sorbents. It was found that the CO_2 adsorption capacity for the samples after modification with APTES was higher than the sorption capacity for unmodified sorbents. The highest sorption capacity reached TiO_2-4 h-120 °C-100 mM-500 °C sample. It was also found that the CO_2 adsorption capacity shows excellent cyclic stability and regenerability after 21 adsorption-desorption cycles.

Keywords: titanium dioxide; 3-aminopropyltriethoxysilane; CO_2 adsorption

Citation: Wanag, A.; Kapica-Kozar, J.; Sienkiewicz, A.; Rokicka-Konieczna, P.; Kusiak-Nejman, E.; Morawski, A.W. Preliminary Findings on CO_2 Capture over APTES-Modified TiO_2. *Atmosphere* **2022**, *13*, 1878. https://doi.org/10.3390/atmos13111878

Academic Editors: Dimitra Karali, Panagiotis Grammelis and Panagiotis Boutikos

Received: 16 September 2022
Accepted: 8 November 2022
Published: 10 November 2022

1. Introduction

Carbon dioxide is one of the most important of Earth's greenhouse gases and its emission is the primary driver of global climate change. It is widely known that to avoid the worst impacts of climate change, the world needs to reduce CO_2 emissions or find a new and efficient method for CO_2 capture or transformation into useful chemical products. CO_2 can be captured by methods and techniques such as chemical absorption, physical adsorption, membrane separation, or chemical looping [1]. Among them, adsorption has become an attractive technology. Qualities of a good adsorbent shall be listed as high adsorption capacity, low cost, high S_{BET} and pore volume as well as long-term stability [2]. Among different sorbents, the most popular are zeolites [3], mesoporous silica [4], porous polymers [5], metal-organic frameworks [6], metal oxide [7] and carbon materials [8]. To improve CO_2 adsorption capacity, surface modification of the sorbents has been studied, including, for example, amine modification [9]. The advantage of amine-modified sorbents is the chemical adsorption between the amine groups and CO_2. Among different amine compounds using to CO_2 adsorbent modification, the most commonly used are tetraethylene pentamine (TEPA) [10–12], monoethanolamine (MEA) [13,14], aminopropyl trialkoxy siliane (APTS) [15,16], Polyethyleneimine (PEI) [17,18].

Titanium dioxide, due to its low cost, chemical inertness, non-toxicity, high oxidation efficiency and photostability, is one of the most promising materials extensively applied in many areas. As one of the most widely used photocatalysts, it is especially applied in the photocatalysis process [19]. However, TiO_2 also finds application as a pigment [20], medical devices coating [21], gas sensors [22], and also as an adsorbent [23]. Furthermore, there are also some publications concerning CO_2 adsorption on the TiO_2 surface [24–26]. Many

efforts have been dedicated to the further improvement of the physico-chemical properties of TiO_2 such as higher S_{BET} and smaller crystallite size of anatase and rutile. In this case, a great deal of modification has been carried out and much attention has especially been paid to the doping of pure TiO_2 with either cations (i.e., Al, Ag, Pt, Co, Fe or Si) or anions (i.e., N, C, I or S) [27]. Currently, one of the promising solutions for the modification of TiO_2 is using silicon. Modification with silicon can increase the specific surface area, reduce particle size, and hinder the anatase-to-rutile phase transition [28,29]. One of the sources of silicon is organosilane coupling agents, for example 3-aminopropyltriethoxysilane (APTES).

Taking the above into account, the present study aimed to prepare APTES-modified titania as a CO_2 adsorbent. Using APTES as a TiO_2 modifier was mainly aimed at improving physico-chemical properties of TiO_2 which have an impact on better CO_2 adsorption. The presented research also determines the influence of the calcination temperature on the structural and adsorption properties of tested materials.

2. Materials and Methods

2.1. Materials and Reagents

The TiO_2used in this study was obtained from slurry titanium dioxide produced by sulphate technology from Chemical Plant Grupa Azoty Zakłady Chemiczne "Police" S.A. (Police, Poland). Before modification, the slurry titanium dioxidewas rinsed with an aqueous solution of ammonia water (25 % pure p.a., Firma Chempur®, Piekary Śląskie, Poland) to remove the residues of sulfuric compounds. This process was thoroughly described in our previous work [30]. As a modifier of TiO_2 was used 3-aminopropyltriethoxysilane (APTES) ($C_9H_{23}NO_3Si$, purity $\geq$ 98%, 221.37 g/mol, Merck KGaA, (Darmstadt, Germany). Ethanol (purity 96%, pure p.a.) purchased from P.P.H. "STANLAB" Sp.J. (Lublin, Poland) was used as a solvent of APTES.

2.2. Synthesis of APTES-Modified TiO_2

The preparation procedure of APTES-modified TiO_2 nanomaterials was described in detail in our previous article [31]. For samples shown in this article, the APTES concentration equals 100 mM. Obtained samples were heated in an argon atmosphere (purity 5.0, Messer Polska Sp. z o.o., Chorzów, Poland) in the GHC 12/900 horizontal furnace (Carbolite Gero, Ltd., Hope, UK). The samples were calcinated at temperatures ranging from 300 °C to 700 °C (Δt = 200 °C) for 4 h. The argon flow was 180 mL/min. After that, the furnace was slowly cooled down to room temperature. Obtained samples are denoted as TiO_2-4 h-120 °C-100 mM-Ar-T, where *T* is the calcination temperature. For comparison, pure TiO_2 was also heated at the same temperature. The reference samples were named TiO_2-Ar-T,where *T* is the calcination temperature.

2.3. Characterization Methods

The prepared nanomaterials were subjected to functional groups analysis using FT-IR-4200 spectrometer (JASCO International Co., Ltd., Tokyo,Japan) equipped with DiffusIR accessory (PIKE Technologies, Fitchburg, USA). The samples were scanned in the spectral range of 4000–400 cm^{-1} with a resolution of 4.0 cm^{-1} averaging 100 scans. X-ray diffraction (XRD) patterns were collected using a powder X-ray diffractometer (Malvern PANalytical Ltd., Malvern, United Kingdom) with Cu Kα radiation (λ = 1.54056 Å). The mean crystallite sizes of the samples were calculated according to Scherrer's equation, while the PDF-4+ 2014 International Centre for Diffraction Data database (04-002-8296 PDF4+ card for anatase and 04-005-5923 PDF4+ card for rutile) was used for identification of the phase composition. TiO_2 anatase over rutile ratio was calculated from [32]:

$$anatase\ content = \frac{1}{1 + 1.26(I_R + I_A)} \quad (1)$$

where I_A and I_R are the diffraction intensities of the (1 0 1) anatase and (1 1 0) rutile crystalline phases at 2θ = 25.3 and 27.4°, respectively.

The S_{BET} surface area and pore volume of nanomaterials were calculated from the nitrogen adsorption-desorption measurements at 77 K carried out in QUADRASORB evo™ Gas Sorption analyzer (Anton Paar GmbH, Graz, Austria). Prior to measurements, all materials were degassed for 16 h at 100 °C under a high vacuum to pre-clean the surface of the tested sample. The single-point value determined the total pore volume from the nitrogen adsorption isotherms at a relative pressure p/p0 = 0.99. Micropore volume was estimated using the Dubinin–Radushkevich method, and mesopore volume was determined as the difference between V_{total} and V_{micro}. Thermogravimetric analysis (TG) and differential thermogravimetry (DTG) was performed in a NETZSCH STA 449 F3 Jupiter (Erich NETZSCH GmbH & Co. Holding KG, Selb, Germany). Samples (about 10 mg) were heated in an open Al_2O_3 crucible with a corresponding empty referent pan. The samples were heated from room temperature to 700 °C at a heating rate of 10 °C/min under a flow of air atmosphere (70 mL/min).

2.4. CO_2 Sorption Measurement

Carbon dioxide adsorption isotherms at 0 °C and 25 °C were measured using QUADRASORB evo™ automatic system (Anton Paar GmbH, Graz, Austria) in the pressure range between 0.01 and 0.98 bar. Before each adsorption experiment, samples were outgassed at 100 °C under a vacuum of 1×10^{-5} mbar for 16 h using a MasterPrep multi-zone flow/vacuum degasser from Quantachrome Instruments (Anton Paar GmbH, Graz, Austria).

The CO_2 adsorption and desorption performance at different temperatures were measured using a NETZSCH STA 449 F3 Jupiter (Erich NETZSCH GmbH & Co. Holding KG, Selb, Germany). An approximately 10 mg sample was placed in an open corundum crucible and pretreated at 105 °C for 60 min under argon flowing at 70 mL/min to remove pre-adsorbed CO_2 and moisture. After 60 min, the argon flow was reduced to 10 mL/min, switched on pure CO_2 and held for 60 min at 30 °C at a flow of 90 mL/min. After adsorption, the gas was switched from CO_2 to argon (70 mL/min), and the temperature increased to 105 °C to desorb the CO_2. Subsequently, the CO_2 adsorption temperature was increased to 40, 50, and 60 °C. After each adsorption measurement, the gas was switched back to pure argon at 70 mL/min to perform desorption at 105 °C for 60 min.

The carbon dioxide cyclic adsorption-desorption measurements were investigated using a thermogravimetric analyzer NETZSCH STA 449 F3 Jupiter (Erich NETZSCH GmbH & Co. Holding KG, Selb, Germany). The CO_2 adsorption was carried out in the same way as described above, with the difference this the measurement of sorption CO_2 was carried out at 21 consecutive adsorption-desorption cycles at the temperature of 30 °C. The CO_2 adsorption capacities were calculated based on the mass gain after CO_2 adsorption regarding the initial sample mass.

3. Results

3.1. Characterization of Materials

The DRIFT spectra of APTES-modified TiO_2 after heat treatment are presented in Figure 1, while reference samples were presented and described in detail in our previous work [33]. The FT-IR/DR spectra present the same bands typical for TiO_2. A wide band from 3700 cm^{-1} to 2500 cm^{-1} is assigned to stretching vibrations of surface –OH groups [34]. As the temperature increases, a decrease in the intensity of these bands can be observed due to the changes in the amount of surface hydroxyl groups [35]. A narrow band at 1620 cm^{-1} is associated with the molecular water bending modes [36]. On all spectra, the presence of the intensive band at around 950 cm^{-1} was found. This band is characteristic of the self-absorption of titania [37]. The characteristic bands from APTES are also noted. The bending and stretching contributions of the alkyl groups [(CH_n)] are located at around 2900 cm^{-1} and 2885 cm^{-1} [38,39]. However, at 1600 cm^{-1} the asymmetric $–NH_3^+$ deformation modes are observed [40,41]. At 1360 cm^{-1}, there is a localized low-intensity band ascribed to C−N bonds [42]. The bands at around 950 cm^{-1} and 920 cm^{-1} are characteristic of the stretching vibrations of Ti–O–Si bonds [43]. These three characteristics of APTES bands are

not observed for samples calcined above 300 °C because they were not permanently bonded to the TiO_2 surface. However, the band at around 1160 cm^{-1} and 1080 cm^{-1} characteristic of the Si−O−Si stretching vibrations and Si–O–C stretching mode, respectively, are noted for all samples [35,44].

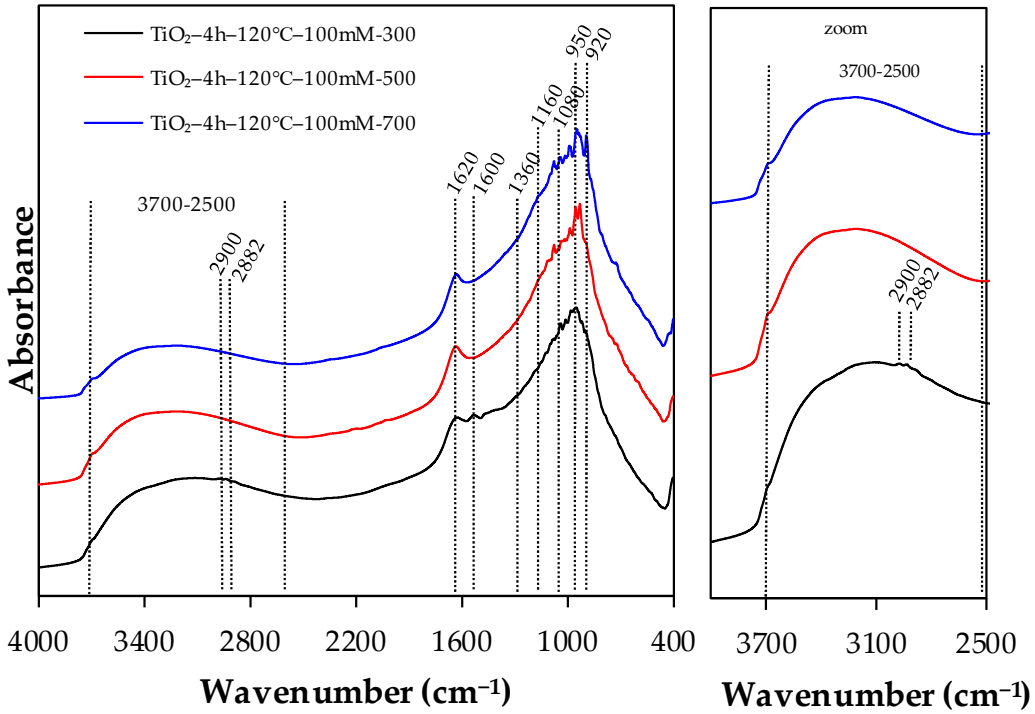

Figure 1. DRIFT spectra of APTES-modified TiO_2 with zoom in wavenumber in the range of 2500–4000 cm^{-1}.

The X-ray diffraction patterns of the APTES-synthesized materials are shown in Figure 2. However, the structural characteristics of reference samples were presented in detail in our previous work [33]. The phase composition and crystallite size of anatase and rutile in all samples are listed in Table 1. According to the data present in Figure 2 and Table 1, all APTES/TiO_2 materials consist mainly of anatase phase (96%) with the characteristic reflections (101), (004), (200), (105), (211), (204), (116), (220), (215) (JCPDS 01-070-7348) located at 25.3, 37.8, 48.1, 53.9, 55.1, 62.7, 68.9, 70.3 and 75.1°, respectively. Some characteristic reflections for rutile phase (110), (101) and (111) (JCPDS 01-076-0318) located at 27.4, 36.0 and 41.2° are also noted. Comparing these results with the results for reference materials, especially the samples calcined at 700 °C (see our previous work [24]), it can be concluded that silicon from APTES had an important influence on the suppression of anatase-to-rutile phase transformation during calcination [45,46]. The influence of silicon on the crystallite size is also observed. For reference materials, the crystallite size was 14–22 nm for anatase and 51->100 nm for rutile, while for APTES-modified TiO_2 samples it was 15–18 nm and 43–73 nm, respectively. Thus, materials heated at the same temperature but after APTES modification are characterized by the smaller crystallites size of both anatase and rutile. Our observation is consistent with results noted by other researchers [28,47]. Silicon can effectively prevent the growth of the crystallites size during calcination.

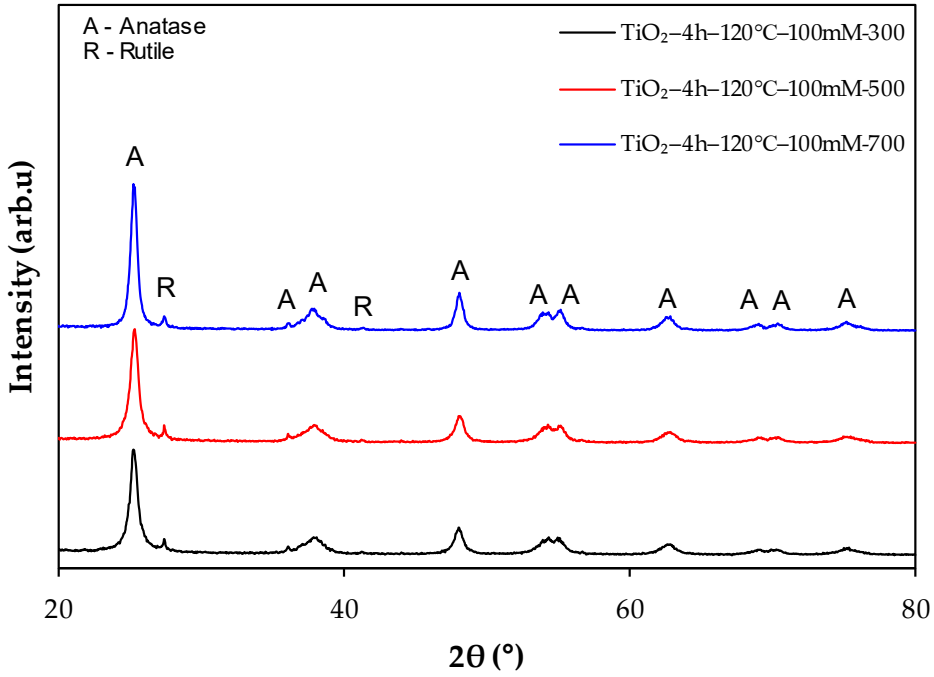

Figure 2. XRD patterns of APTES-modified TiO_2.

Table 1. XRD phase composition and average crystallite size of APTES-modified TiO_2 as well as reference samples.

Sample Name	Anatase in Crystallite Phase [%]	Anatase Crystallite Size [nm]	Rutile in Crystallite Phase [%]	Rutile Crystallite Size [nm]
TiO_2-Ar-300 °C	96	14	4	51
TiO_2-Ar-500 °C	95	18	5	41
TiO_2-Ar-700 °C	88	22	12	>100
TiO_2-4 h-120 °C-100 mM-300 °C	96	15	4	46
TiO_2-4 h-120 °C-100 mM-500 °C	96	15	4	45
TiO_2-4 h-120 °C-100 mM-700 °C	96	18	4	73

The specific surface area and total pore volume are listed in Table 2. Based on the presented data, all tested APTES synthesized samples are mesoporous materials. Only the TiO_2-Ar-700 °C sample is microporous. The increase in calcination temperature from 300 to 700 °C significantly reduced specific surface area and pore size distribution. The S_{BET} of the samples decreases from 178 m^2/g at 300 °C to 108 m^2/g at 700 °C, respectively. It is a typical phenomenon due to the sintering and aggregation of TiO_2 particles during temperature modification [48]. However, it should be noted that samples after modification show significantly higher S_{BET} than reference samples due to the effective inhibition of the growth of the crystallite size of TiO_2 by silicon presence in samples after APTES modification.

The thermal analysis TG/DTG profiles of the unmodified and APTES-modified samples are illustrated in Figures 3a,b and 4a,b. As can be seen from the recorded curves, the total weight loss for the unmodified samples decreases with increasing calcination temperature reaching 1.95, 1.77 and 0.52%, which is accompanied by the decomposition peaks screened between 30–210 °C, reaching the maximum amount with the DTG peak at ca. 96, 128 and 149 °C, respectively. This mass change is attributed to the vaporization of free water and water bonded to the cations by hydrogen bonding [49,50]. At the temperature range of 200–390 °C, we observed that a second weight loss can be correlated with the anatase-to-rutile transformation [51]. In the case of the APTES-modified sample (Figure 4a,b), we can also observe a mass change which is attributed to the removal of

physically adsorbed water in the temperature range of 30–170 °C at the maximum at above 90 °C, reaching a weight loss of 3.85, 2.56 and 1.77% for the TiO_2-4 h-120-100 mM-300, TiO_2-4 h-120-100 mM-500 and TiO_2-4 h-120-100 mM-700, respectively.

Table 2. Specific surface area andpore volume distribution ofAPTES-modified TiO_2 as well as reference samples.

Sample Name	S_{BET} [m^2/g]	V_{total} [a] [cm^3/g]	V_{micro} [b] [cm_3/g]	V_{meso} [c] [cm^3/g]	CO_2 Adsorption at 0 °C [mmol/g]	CO_2 Adsorption at 25 °C [mmol/g]
TiO_2-Ar-300 °C	112	0.31	0.04	0.27	0.36	0.25
TiO_2-Ar-500 °C	75	0.22	0.03	0.19	0.36	0.16
TiO_2-Ar-700 °C	23	0.10	0.01	0.09	0.09	0.07
TiO_2-4 h-120 °C-100 mM-300 °C	178	0.26	0.06	0.20	0.47	0.29
TiO_2-4 h-120 °C-100 mM-500 °C	153	0.28	0.06	0.22	0.56	0.29
TiO_2-4 h-120 °C-100 mM-700 °C	108	0.27	0.04	0.23	0.33	0.15

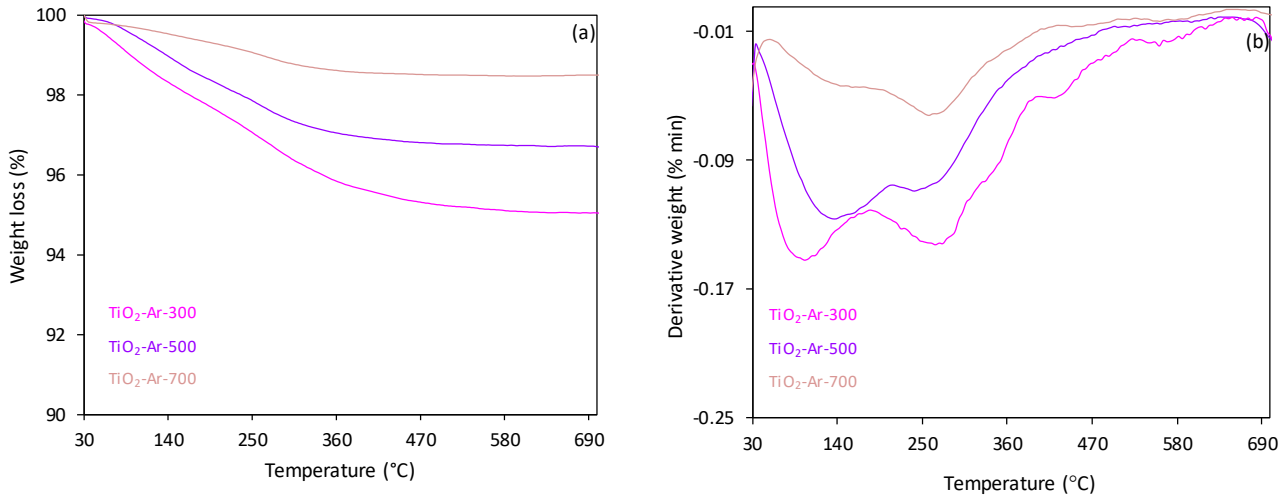

Figure 3. (**a**) TG and (**b**) DTG curves of the unmodified samples calcined at various temperatures.

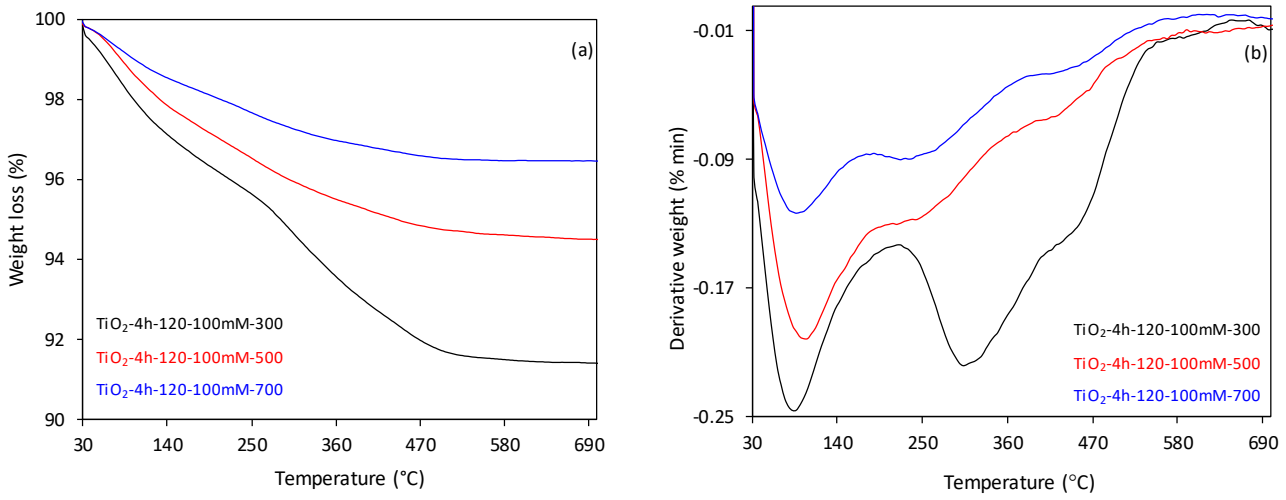

Figure 4. (**a**) TG and (**b**) DTG curves of the APTES modified nanomaterials.

Additionally, the strong decomposition peaks between the 200–390 °C for the TiO_2-4 h-120-100 m-300 samples, corresponding to the differential thermogravimetric (DTG) profile

with a maximum at 310 °C and the total weight loss reached 3.25%, respectively, is observed. These decomposition peaks could be attributed to the adsorbed silanes hydrogen bonded to the surface hydroxyl groups [52–54]. In the case of samples TiO_2-4 h-120-100 m-500 and TiO_2-4 h-120-100 m-700, we can note much less sharp but wider decomposition peaks at the same temperature range. It is also worth noticing that the increase in the calcination temperature of APTES-modified TiO_2 samples results in a decrease in the total weight loss from 1,65% and 1,28% for the TiO_2-4 h-120-100 mM-500 and TiO_2-4 h-120-100 m-700 samples, respectively. It can be explained as follows: during the calcination, free silanol on the surface was dehydrated and translated into hydrogen-bonded silanol [46]. Furthermore, the results also show that as the calcining temperature increases, the initial and maximum rate decomposition (DTG profile) temperature shifted towards lower values, reaching the maximum at ca. 196 and 263 °C for TiO_2-4 h-120-100 m-500 and 243 °C for TiO_2-4 h-120-100 m-700 samples. The last decomposition reaction, which occurs between 400–550 °C, reaches the maximum at 438 °C (DTG profile) and the total weight losses of 1.30%, 0.90% and 0.47% for the samples calcined with 300, 500 and 700 °C, respectively, are due to the chemically grafted silane [55].

3.2. CO_2 Adsorption Properties

The calculated values of carbon dioxide adsorption capacity at 0 °C for the samples calcined with the various temperatures before and after modification via APTES are summarized in Table 2 and graphically shown in Figure 5a,b. Similar values of the CO_2 adsorption capacity (0.36 mmol/g) at 0 °C for an unmodified material were noticed for the samples calcined at 300 °C and 500 °C. The adsorption capacity drastically decreased to 700 °C with the temperature calcination increase and reached 0.09 mmol/g. The decrease in the sorption capacity with the increase in the calcination temperature can be explained by considering the properties of the porous structure of the samples (Table 1). The specific surface area (S_{BET}), total pore volume (V_{total}) and mesopore volume (V_{meso}) for TiO_2-Ar-300 and TiO_2-Ar-500 was 112 m^2/g, 0.31 cm^3/g, 0.23 cm^3/g and 75 m^2/g 0.22 cm^3/g, 0.19 cm^3/g, respectively. In the case of the sample calcined at 700 °C (TiO_2-Ar-700), the specific surface area decreased to 23 m^2/g, and total pore volume and mesopore volume decreased to 0.10 cm^3/g and 0.01 cm^3/g, accordingly.

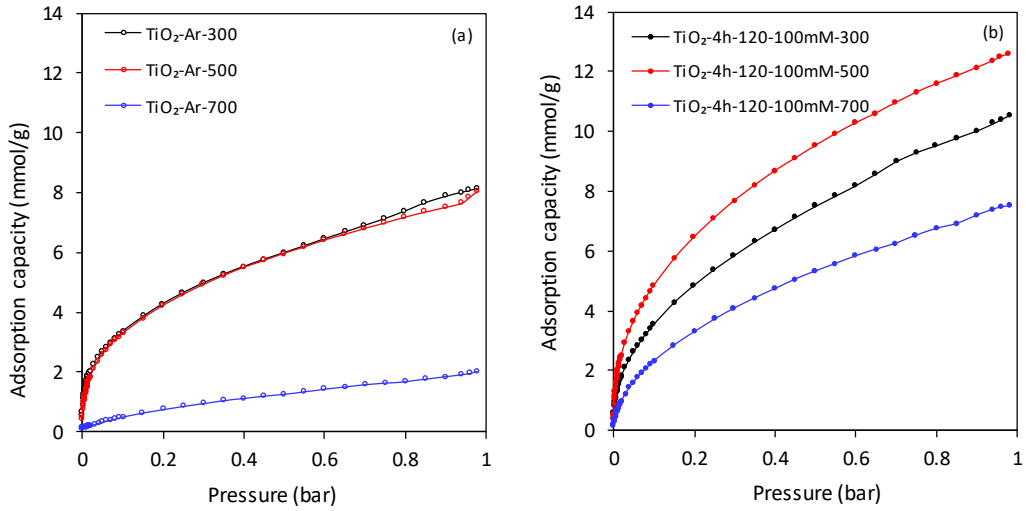

Figure 5. CO_2 adsorption capacity recorded at 0 °C of (**a**) unmodified samples and (**b**) samples modified with APTES calcined at various temperatures.

The sorption capacity changed significantly after modification via APTES and reached for TiO_2-4 h-120-100 mM-300, TiO_2-4 h-120-100 mM-500 and TiO_2-4 h-120-100 mM-700 0.47 mmol/g, 0.56 mmol/g, 0.33 mmol/g and it is 29%, 56% and 272%, respectively, higher than the same samples before being modified with APTES (Figure 5b). Moreover, we can

see that the modification process leads to a significant increase in the structural parameters. The specific surface area increased to 178 m^2/g for the TiO_2-4 h-120-100 mM-300 sample, TiO_2-4 h-120-100 mM-500 and TiO_2-4 h-120-100 mM-700 samples increased to 153 m^2/g and 108 m^2/g, respectively, that is 1.6, 2.0 and 4.7 times higher than the same samples before APTES-modified.

The APTES-modified TiO_2 samples were selected for CO_2 sorption at different temperatures due to higher CO_2 sorption capacity at 0 °C compared to unmodified samples. The results of these experiments are presented in Figure 6. The sorption results at 30, 40, 50 and 60 °C show the same tendency that occurs in the adsorption at 0 °C. From the graph, it can be observed that the effect of increasing the temperature is to decrease the adsorption capacity (what was expected) because it is typical behavior showing the effect of temperature on CO_2 adsorption. For instance, the highest CO_2 sorption capacity at 30 °C (0.30 mmol/g) exhibited TiO_2-4 h-120-100 mM-500 sample, then sorption capacity it reduces by 0,04 mmol/g, 0,06 mmol/g and 0,11 mmol/g when the adsorption temperature increased from 40 °C to 60 °C. This corresponds to an 8%, 12% and 16% decrease compared to the CO_2 adsorption capacity at 30 °C. This can be explained by the fact that an increase in adsorption temperature stands for high gas molecule energy. Increasing energy allows gaseous molecules to diffuse at a greater rate, in turn reducing the chance for the CO_2 to be restrained or trapped by fixed energy adsorption sites on the adsorbent surface [56–59].

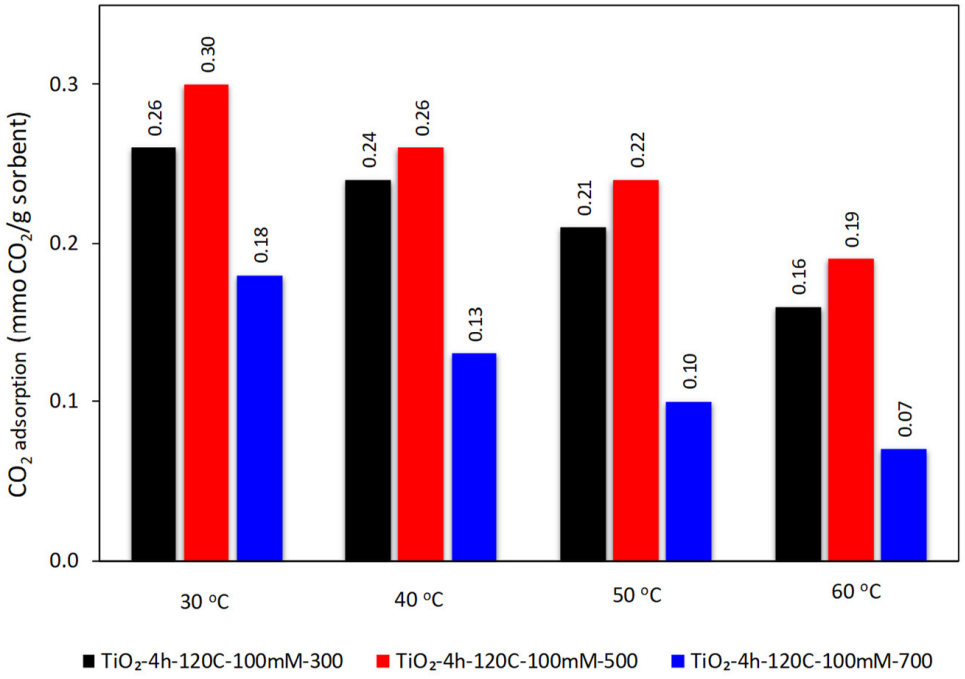

Figure 6. Temperature dependence of CO_2 adsorption capacity.

The cyclic adsorption-desorption behavior was carried out for the TiO_2-4 h-120-100 mM-500 sample that achieved the highest CO_2 sorption capacity at both 0 °C and 30, 40, 50 and 60 °C among all APTES-modified TiO_2 samples and calcined with various temperatures. The calculated CO_2 capacities during twenty-one consecutive adsorption-desorption cycles at 30 °C are shown in Figure 7. It could be seen that the CO_2 adsorption capacity shows excellent cyclic stability and regenerability after 21 adsorption-desorption cycles, which is crucial for practical application.

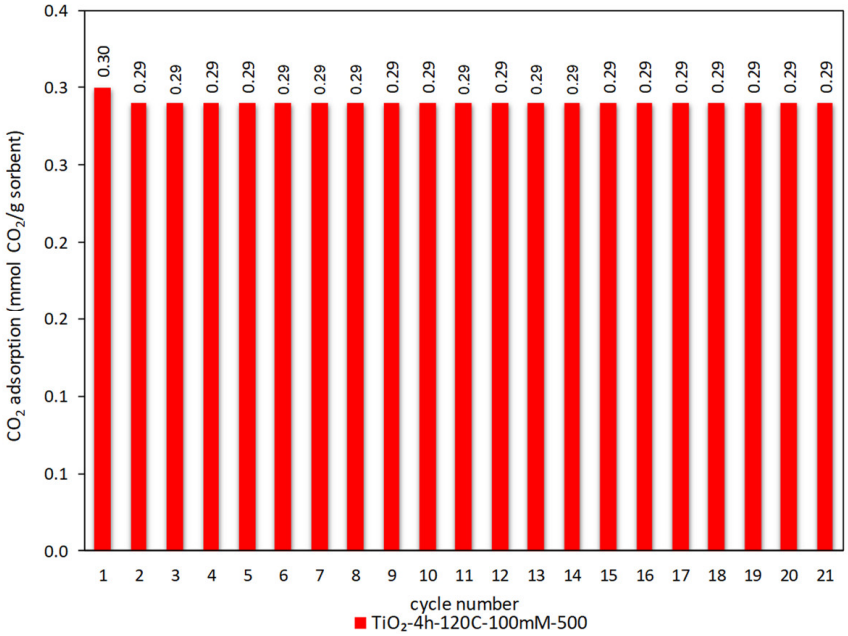

Figure 7. Cyclic stability of CO_2 adsorption-desorption for a TiO_2-4 h-120-100 mM-500 sample at 30 °C.

4. Conclusions

APTES-modified TiO_2 nanomaterials for CO_2 adsorption were successfully prepared. The materials were obtained by solvothermal process and thermal modification in the argon atmosphere at different temperatures (from 300 °C to 700 °C). It was confirmed that silicon can effectively prevent titania grains' growth during calcination and suppress the decreases in $S_{BET}$and the pore size of samples. Furthermore, it was found that these parameters had an essential influence on the CO_2 adsorption properties of studied materials. After modification via APTES, the sorption capacity of samples was significantly changed and was 29%, 56% and 272% higher than the samples without modification with APTES. The highest sorption capacity reached TiO_2-4 h-120 °C-100 mM-500 °C sample. For this material, the CO_2 adsorption capacity also shows excellent cyclic stability and regenerability after 21 adsorption-desorption cycles, which are crucial for practical application.

Author Contributions: Conceptualization: A.W. and J.K.-K.; investigation: A.W., J.K.-K. and A.S.; data curation: E.K.-N. and A.W.M.; writing—original draft preparation: A.W. and J.K.-K.; writing—review and editing: A.W.M., E.K.-N. and P.R.-K.; project administration: A.W.M.; funding acquisition: A.W.M. All authors have read and agreed to the published version of the manuscript.

Funding: This work was supported by grant 2017/27/B/ST8/02007 from the National Science Centre, Poland.

Institutional Review Board Statement: Not applicable.

Informed Consent Statement: Not applicable.

Data Availability Statement: The data presented in this study are available on request from thecorresponding author.

Conflicts of Interest: The authors declare no conflict of interest.

References

1. Madejski, P.; Chmiel, K.; Subramanian, N.; Kús, T. Methods and techniques for CO_2 capture: Review of potential solutions and applications in modern energy technologies. *Energies* **2022**, *15*, 887. [CrossRef]
2. Abuelnoor, N.; AlHajaj, A.; Khaleel, M.; Vega, L.F.; Abu-Zahra, M.R.M. Activated carbons from biomass-based sources for CO_2 capture applications. *Chemosphere* **2021**, *282*, 131111. [CrossRef]

3. Lee, J.S.; Kim, J.H.; Kim, J.T.; Suh, J.K.; Lee, J.M.; Lee, C.H. Adsorption equilibria of CO_2 on zeolite 13X and zeolite X/Activated carbon composite. *J. Chem. Eng. Data* **2002**, *47*, 1237–1242. [CrossRef]
4. Zhao, G.; Aziz, B.; Hedin, N. Carbon dioxide adsorption on mesoporous silica surfaces containing amine-like motifs. *Appl. Energy* **2010**, *87*, 2907–2913. [CrossRef]
5. Liao, Y.; Cheng, Z.; Trunk, M.; Thomas, A. Targeted control over the porosities and functionalities of conjugated microporous polycarbazole networks for CO_2-selective capture and H_2 storage. *Polym. Chem.* **2017**, *8*, 7240–7247. [CrossRef]
6. Kang, M.; Kim, J.E.; Kang, D.W.; Lee, H.Y.; Moon, D.; Hong, C.S. A diamine-grafted metal–organic framework with outstanding CO_2 capture properties and a facile coating approach for imparting exceptional moisture stability. *J. Mater. Chem. A* **2019**, *7*, 8177–8183. [CrossRef]
7. Guo, B.; Wang, Y.; Qiao, X.; Shen, X.; Guo, J.; Xiang, J.; Jin, Y. Experiment and regeneration kinetic model study on CO_2 adsorbent prepared from fly ash. *Chem. Eng. J.* **2020**, *421*, 127865. [CrossRef]
8. Siriwardane, R.V.; Shen, M.S.; Fisher, E.P.; Poston, J.A. Adsorption of CO_2 on molecular sieves and activated carbon. *Energy Fuels* **2001**, *15*, 279–284. [CrossRef]
9. Chen, C.; Kim, J.; Ahn, W.S. CO_2 capture by amine-functionalized nanoporous materials: A review. *Korean J. Chem. Eng.* **2014**, *31*, 1919–1934. [CrossRef]
10. Knöfel, C.; Descarpentries, J.; Benzaouia, A.; Zeleňák, V.; Mornet, S.; Llewellyn, P.L.; Hornebecq, V. Functionalised micro-/mesoporous silica for the adsorption of carbon dioxide. *Microporous Mesoporous Mater.* **2007**, *99*, 79–85. [CrossRef]
11. Wang, Y.; Guo, T.; Hu, X.; Hao, J.; Guo, Q. Mechanism and kinetics of CO_2 adsorption for TEPA- impregnated hierarchical mesoporous carbon in the presence of water vapour. *Powder Technol.* **2020**, *368*, 227–236. [CrossRef]
12. Kapica-Kozar, J.; Michalkiewicz, B.; Wrobel, R.J.; Mozia, S.; Piróg, E.; Kusiak-Nejman, E.; Serafin, J.; Morawski, A.W.; Narkiewicz, U. Adsorption of carbon dioxide on TEPA-modified TiO_2/titanate composite nanorods. *New J. Chem.* **2017**, *41*, 7870–7885. [CrossRef]
13. Luis, P. Use of monoethanolamine (MEA) for CO_2 capture in a global scenario: Consequences and alternatives. *Desolination* **2016**, *380*, 93–99. [CrossRef]
14. Ünveren, E.E.; Monkul, B.Ö.; Sarıoğlan, Ş.; Karademir, N.; Alper, E. Solid amine sorbents for CO_2 capture by chemical adsorp-tion: A review. *Petroleum* **2017**, *3*, 37–50. [CrossRef]
15. Knowles, G.P.; Chaffee, A.L. Aminopropyl-functionalized silica CO_2 adsorbents via sonochemical methods. *J. Chem.* **2016**, *2016*, 070838. [CrossRef]
16. Su, F.; Lu, C.H.; Cnen, W.; Bai, H.; Hwang, J.F. Capture of CO_2 from flue gas via multiwalled carbon nanotubes. *Sci. Total Environ.* **2009**, *407*, 3017–3023. [CrossRef]
17. Jeon, S.; Min, J.; Kim, S.H.; Lee, K.B. Introduction of cross-linking agents to enhance the performance and chemical stability of polyethyleneimine-impregnated CO_2 adsorbents: Effect of different alkyl chain lengths. *Chem. Eng. J.* **2020**, *398*, 125531. [CrossRef]
18. Ahmed, S.; Ramli, A.; Yusup, S. Development of polyethylenimine-functionalized mesoporous Si-MCM-41 for CO_2 adsorption. *Fuel Process Technol.* **2017**, *167*, 622–630. [CrossRef]
19. Fujishima, A.; Zhang, X.; Tryk, D.A. TiO_2 photocatalysis and related surface phenomena. *Surf. Sci. Rep.* **2008**, *63*, 515–582. [CrossRef]
20. Feldmann, C. Preparation of nanoscale pigment particles. *Adv. Mater.* **2001**, *13*, 1301. [CrossRef]
21. Ferrari, M. Cancer nanotechnology: Opportunities and challenges. *Nat. Rev. Cancer.* **2005**, *5*, 161. [CrossRef] [PubMed]
22. Chen, N.; Lib, Y.; Deng, D.; Liu, X.; Xing, X.; Xiao, X.; Wang, Y. Acetone sensing performances based on nanoporous TiO_2 sy,nthesized by a facile hydrothermal method Sensor. *Actuator. B Chem.* **2017**, *238*, 238491–238500. [CrossRef]
23. Wanbayor, R.; Ruangpornvisuti, V. Adsorption of di-, tri- and polyatomic gases on the anatase TiO_2 (0 0 1) and (1 0 1) surfaces an,d their adsorption abilities. *J. Mol. Stuct.* **2010**, *952*, 103–108. [CrossRef]
24. Aquino, C.C.; Richner, G.; Kimling, M.C.; Chen, D.; Puxty, G.; Feron, P.H.M.; Caruso, R.A. Amine-functionalized titania-based po,rous structures for carbon dioxide postcombustion capture. *J. Phys. Chem. C.* **2013**, *117*, 9747–9757. [CrossRef]
25. Muller, K.; Lu, D.; Senanayake, S.D.; Starr, D.E. Monoethanolamine adsorption on TiO_2(110): Bonding, structure, and implications for use as a model solid-supported CO_2 capture material. *J. Phys. Chem. C.* **2014**, *18*, 1576–1586. [CrossRef]
26. Kapica-Kozar, J.; Pirog, E.; Kusiak-Nejman, E.; Wrobel, R.J.; Gesikiewicz-Puchalska, A.; Morawski, A.W.; Nakiewicz, U.; Michalkiewicz, B. Titanium dioxide modified with various amines used as sorbents of carbon dioxide. *New J. Chem.* **2017**, *41*, 1549–1557. [CrossRef]
27. Daghrir, R.; Drogui, P.; Robert, D. Modified TiO_2 for environmental photocatalytic applications: A review. *Ind. Eng. Chem. Res.* **2013**, *52*, 3581–3599. [CrossRef]
28. Xu, G.Q.; Zheng, Z.X.; Wu, Y.C.; Feng, N. Effect of silica on the microstructure and photocatalytic properties of titania. *Ceram. Int.* **2009**, *35*, 1–5. [CrossRef]
29. Tobaldi, D.M.; Tucci, A.; Skapin, A.S.; Esposito, L. Effects of SiO_2 addition on TiO_2 crystal structure and photocatalytic activity. *J. Eur. Ceram. Soc.* **2010**, *30*, 2481–2490. [CrossRef]
30. Kusiak-Nejman, E.; Wanag, A.; Kapica-Kozar, J.; Morawski, A.W. Preparation and characterisation of TiO_2 thermally modified with cyclohexane vapours. *Int. J. Mater. Prod. Techn.* **2016**, *52*, 286–297. [CrossRef]

31. Wanag, A.; Sienkiewicz, A.; Rokicka-Konieczna, P.; Kusiak-Nejman, E.; Morawski, A.W. Influences of modification of titanium dioxide by silane coupling agents on the photocatalytic activity and stability. *J. Environ. Chem. Eng.* **2020**, *8*, 103917. [CrossRef]
32. Colón, G.; Sánchez-España, J.M.; Hidalgo, M.C.; Navío, J.A. Effect of TiO_2 acidic pre-treatment on the photocatalytic properties for phenol degradation. *J. Photochem. Photobiol. A* **2006**, *179*, 20–27. [CrossRef]
33. Sienkiewicz, A.; Wanag, A.; Kusiak-Nejman, E.; Ekiert, E.; Rokicka-Konieczna, P.; Morawski, A.W. Effect of calcination on the photocatalytic activity and stability of TiO_2 photocatalysts modified with APTES. *J. Environ. Chem. Eng.* **2021**, *9*, 104794. [CrossRef]
34. Winter, M.; Hamal, D.; Yang, X.; Kwen, H.; Jones, D.; Rajagopalan, S.H.; Klabunde, K.J. Defining reactivity of solid sorbents: What is the most appropriate metric? *Chem. Mater.* **2009**, *21*, 2367–2374. [CrossRef]
35. Haque, F.Z.; Nandanwar, R.; Singh, P. Evaluating photodegradation properties of anatase and rutile TiO_2 nanoparticles for organic compounds. *Optik* **2017**, *128*, 191–200. [CrossRef]
36. Cheng, F.; Sajedin, S.M.; Kelly, S.M.; Lee, A.F.; Kornherr, A. UV-stable paper coated with APTES-modified P25 TiO_2 nanoparticles. *Carbohydr. Polym.* **2016**, *114*, 246–252. [CrossRef]
37. Maira, A.J.; Coronado, J.M.; Augugliaro, V.; Yeung, K.L.; Conesa, J.C.; Soria, J. Fourier transform infrared study of the performance of nanostructured TiO_2 particles for the photocatalytic oxidation of gaseous toluene. *J. Catal.* **2001**, *202*, 413–420. [CrossRef]
38. Saliba, P.A.; Mansur, A.A.P.; Mansur, H.S. Advanced nanocomposite coatings of fusion bonded epoxy reinforced with amino-functionalized nanoparticles for applications in underwater oil pipelines. *J. Nanomater.* **2016**, *2016*, 7281726. [CrossRef]
39. Shakeri, A.; Yip, D.; Badv, M.; Imani, S.M.; Sanjari, M.; Didar, T.F. Self-cleaning ceramic tiles produced via stable coating of TiO_2 nanoparticles. *Materials* **2018**, *11*, 1003. [CrossRef]
40. Razmjou, A.; Mansouri, J.; Chena, V. The effects of mechanical and chemical modification of TiO_2 nanoparticles on the surface chemistry, structure and fouling performance of PES ultrafiltration membranes. *J. Membr. Sci.* **2011**, *378*, 73–84. [CrossRef]
41. Ukaji, E.; Furusawa, T.; Sato, M.; Suzuki, M. The effect of surface modification with silane coupling agent on suppressing the photo-catalytic activity of fine TiO_2 particles as inorganic UV filter. *Appl. Surf. Sci.* **2007**, *254*, 563–569. [CrossRef]
42. Youssef, Z.; Jouan-Hureaux, V.; Colombeau, L.; Arnoux, P.; Moussaron, A.; Baros, F.; Toufaily, J.; Harmieh, T.; Roques-Carmes, T.; Frochot, C. Titania and silica nanoparticles coupled to Chlorin e6 for anti-cancer photodynamic therapy. *Photodiagnosis Photodyn. Ther.* **2018**, *22*, 115–126. [CrossRef] [PubMed]
43. Gao, X.; Wachs, I.E. Titania-silica as catalysts: Molecularstructural characteristics and physico-chemical properties. *Catal. Today* **1999**, *51*, 233–254. [CrossRef]
44. Milanesi, F.; Cappelletti, G.; Annunziata, R.; Bianchi, C.L.; Meroni, D.; Ardizzone, S. Siloxane-TiO_2 hybrid nanocomposites. The structure of the hydrophobic layer. *J. Phys. Chem. C* **2010**, *114*, 8287–8293. [CrossRef]
45. Dalod, A.R.M.; Henriksen, L.; Grande, T.; Einarsrud, M.-A. Functionalized TiO_2 nanoparticles by single-step hydrothermal synthesis: The role of the silane coupling agents. *Beilstein, J. Nanotechnol.* **2017**, *8*, 304–312. [CrossRef]
46. Okada, K.; Yamamoto, N.; Kameshima, Y.; Yasumori, A.; MacKenzie, K.J.D. Effect of silica additive on the anatase-to-rutile phase transition. *Ceram. Soc.* **2001**, *84*, 1591–1596. [CrossRef]
47. Cheng, P.; Zheng, M.; Jin, Y.; Huang, Q.; Gu, M. Preparation and characterization of silica-doped titania photocatalyst through sol–gel method. *Mater. Lett.* **2003**, *57*, 2989–2994. [CrossRef]
48. Wong, Y.C.; Tan, Y.P.; Taufiq-Yap, Y.H.; Ramli, I. Effect of calcination temperatures of CaO/Nb_2O_5 mixed oxides catalysts on biodiesel production. *Sains Malays.* **2014**, *43*, 783–790.
49. Galaburdaa, M.V.; Bogatyrova, V.M.; Skubiszewska-Zieba, J.; Oranskaa, O.I.; Sternik, D.; Gun'ko, V.M. Synthesis and structural features of resorcinol-formaldehyde resin chars containing nickel nanoparticles. *Appl. Surf. Sci.* **2016**, *360*, 722–730. [CrossRef]
50. Xie, W.; Gao, Z.; Pan, W.P.; Hunter, D.; Singh, R.A. Vaia, Thermal degradation chemistry of alkyl quaternary ammonium montmorillonite. *Chem. Mat.* **2001**, *13*, 2979–2990. [CrossRef]
51. Chen, G.; Chen, J.; Song, Z.; Srinivasakannan, C.; Peng, J. A new highly efficient method for the synthesis of rutile TiO_2. *J. Alloys Compd.* **2014**, *585*, 75–77. [CrossRef]
52. Nakonieczny, D.S.; Kern, F.; Dufner, L.; Dubiel, A.; Antonowicz, M.; Matus, K. Effect of calcination temperature on the phase composition, morphology, and thermal properties of ZrO_2 and Al_2O_3 modified with APTES (3-aminopropyltriethoxysilane). *Materials* **2021**, *14*, 6651. [CrossRef] [PubMed]
53. Yuan, P.; Southon, P.D.; Liu, Z.; Green, M.E.R.; Hook, J.M.; Antill, S.J.; Kepert, C.J. Functionalization of halloysite clay nanotubes by grafting with γ-aminopropyltriethoxysilane. *J. Phys. Chem. C.* **2008**, *112*, 15742–15751. [CrossRef]
54. Shanmugharaj, A.M.; Rhee, K.Y.; Ryu, S.H. Influence of dispersing medium on grafting of aminopropyltriethoxysilane in swelling clay materials. *J. Colloid Interface Sci.* **2006**, *298*, 854–859. [CrossRef] [PubMed]
55. Asgari, M.; Sundararaj, U. Silane functionalization of sodium montmorillonite nanoclay: The effect of dispersing media on intercalation and chemical grafting. *Appl. Clay Sci.* **2018**, *153*, 228–238. [CrossRef]
56. Zhou, L.; Fan, J.; Cui, G.; Shang, X.; Tang, Q.; Wang, J.; Fan, M. Highly efficient and reversible CO_2 adsorption by amine-grafted platelet SBA-15 with expanded pore diameters and short mesochannels. *Green Chem.* **2014**, *16*, 4009–4016. [CrossRef]
57. Fauth, D.J.; Gray, M.L.; Pennline, H.W. Investigation of porous silica supported mixed-amine sorbents for post-combustion CO_2 capture. *Energy Fuels* **2012**, *26*, 2483–2496. [CrossRef]

58. Zhang, L.; Aziz, N.; Ren, T.; Wang, Z. Influence of Temperature on the Gas Content of Coal and Sorption Modelling 2011 Underground Coal Operators Conference. Available online: https://ro.uow.edu.au/coal/367/ (accessed on 1 November 2022).
59. Hauchhum, L.; Mahanta, P.R. Carbon dioxide adsorption on zeolites and activated carbon by pressure swing adsorption in a fixed bed. *Int. J. Energy Environ. Eng.* **2014**, *53*, 49–356. [CrossRef]